Quantitative SAXS Analysis of the P123/Water/Ethanol Ternary Phase Diagram

S. S. Soni,[†] G. Brotons,[†] M. Bellour,[†] T. Narayanan,[‡] and A. Gibaud*[,†]

Laboratoire de Physique de l'Etat Condensé (LPEC), Faculté des Sciences, Université du Maine, UMR 6087 CNRS, 72085 Le Mans, Cedex 09, France, and European Synchrotron Radiation Facility (ESRF), BP 220, 38043 Grenoble Cedex, France

Received: April 6, 2006; In Final Form: June 3, 2006

The ternary phase diagram of the amphiphilic triblock copolymer PEO−PPO−PEO ($(EO)_{20}(PO)_{70}(EO)_{20}$ commercialized under the generic name P123), water, and ethanol has been investigated at constant temperature ($T = 23$ °C) by small-angle X-ray scattering (SAXS). The microstructure resulting from the self-assembly of the PEO−PPO−PEO block copolymer varies from micelles in solution to various types of liquid crystalline phases such as cubic, 3D hexagonal close packed spheres (HCPS), 2D hexagonal, and lamellar when the concentration of the polymer is increased. In the isotropic liquid phase, the micellar structural parameters are obtained as a function of the water−ethanol ratio and block copolymer concentration by fitting the scattering data to a model involving core−shell form factor and a hard sphere structure factor of interaction. The micellar core, the aggregation number, and the hard sphere interaction radius decrease when increasing the ethanol/water ratio in the mixed solvent. We show that the fraction of ethanol present in the core is responsible for the swelling of the PPO blocks. In the different liquid crystalline phases, structural parameters such as lattice spacing, interfacial area of PEO block, and aggregation number are also evaluated. In addition to classical phases such as lamellar, 2D hexagonal, and liquid isotropic phases, we have observed a two-phase region in which cubic $Fm3m$ and $P6_3mmc$ (hexagonally close packing of spheres (HCPS)) phases coexist. This appears at 30% (w/w) of P123 in pure water and with 5% (w/w) of ethanol. At 10% (w/w) ethanol, only the HCPS phase remains present.

1. Introduction

Poly(ethylene oxide)−poly(propylene oxide)−poly(ethylene oxide) PEO−PPO−PEO block copolymers (commercially available as Poloxamers or Pluronics) is a class of block copolymers very promising not only in material science but also for pharmaceutical applications.[1,2] Aggregates of PEO−PPO−PEO block copolymers in water have been studied in the past with the aim to examine their associative properties. Indeed they exhibit a wealth of different phases depending on the block copolymer molecular weight and PEO/PPO block ratio, the solvent type, and more importantly, the block copolymer/solvent composition.[3−13] After the discovery of the MCM41 hybrid mesophases in 1992 by the Mobil Corporation researchers, synthetic surfactants such as CTAB have been extensively studied for their structuring properties. More recently, triblock copolymers and in particular Pluronics such as P123 and F127 have also been used as templating agents for the design of highly organized oxide materials by sol−gel chemistry.[14−16] Thin films of such materials are widely studied nowadays because of their potential applications in the design of low-*k* dielectrics coatings, for catalysis or sensors. Their fabrication can be obtained following the evaporation induced self-assembly (EISA) route which is based on the rapid evaporation of an organic solvent (usually ethanol) promoting the 2D or 3D self-assembly of the surfactant and the simultaneous condensation of the inorganic oxide precursor.[17−20] The formation of well-organized structures by EISA is observed in the very last moments of the evaporation, when the surfactant is mainly in contact with water and when little amounts of ethanol remain in the solution. To get a better understanding of such a process and of the parameters that influence the formation and the properties of these films, it is crucial to investigate the phase diagram of triblock copolymers in the presence of selective solvents such as water and ethanol.

In this paper, we report the determination of the ternary phase diagram of the system P123/water/ethanol by small-angle X-ray scattering (SAXS). The binary phase diagram of P123 with water has been reported by Wanka et al.[4] It presents isotropic, cubic, 2D hexagonal, and lamellar phases in a large range of temperatures. Recently Ganguly et al.[21] reported the effect of the addition of NaCl and ethanol on the P123/water system in the diluted isotropic phase by using small angle neutron scattering (SANS) and dynamic light scattering (DLS). Here at room temperature (fixed at $T = 23$ °C), we show how the presence of ethanol modifies the phases formed from the diluted ones to the more concentrated lamellar phase. SAXS curves were quantitatively analyzed at each composition. In the isotropic dilute liquid phase, the data were fitted with a model of interacting polydisperse micelles. In the crystalline phases, the peak positions were indexed, and the corresponding structural parameters and space group are presented.

2. Experimental Section

P123, namely $(EO)_{20}(PO)_{70}(EO)_{20}$ purchased from Aldrich was used as received with a specified average molecular weight of 5800. Samples were prepared in sealed vials by adjusting the mass of P123, water, and ethanol at each composition.

* To whom correspondence should be addressed. E-mail: alain.gibaud@univ-lemans.fr. Fax: (33) 243 833 518.

[†] Université du Maine.

[‡] European Synchrotron Radiation Facility.

10.1021/jp062159p CCC: $33.50
Published on Web 07/18/2006

Deionized water and 99.8% pure ethanol were used. To promote the easy dissolution of the surfactant, P123 was heated at 40 °C prior to mixing it with ethanol and water. Solutions were then stored at ambient temperature for several weeks before the measurements. The phase diagram was established for the ethanol mass fraction lower than 20% (w/w). Fluid liquid mixtures were inserted in 1 mm glass capillaries, whereas gels were mounted in an aluminum cell having transparent windows.

SAXS measurements were carried out at the ID02 beam line,[22] ESRF in Grenoble, France. The incident X-ray wavelength (λ) was 0.996 Å, and the scattered intensity was recorded by an image intensified CCD detector placed at 3 m from the sample. Measurements covered a scattering vector (q) range of $0.06 < q < 2$ nm^{-1}, and the typical acquisition time was in the range of 100 ms. The 2D SAXS patterns were normalized and regrouped to 1D scattering curves using the standard procedure. The background scattering by the solvent (mainly water) and the sample holder was subtracted from the normalized sample scattering, and the resulting quantity is denoted as scattering cross-section. Before presenting the results, we first discuss the theoretical approach of our data analysis.

3. Theoretical Approach of SAXS Results

3.1. Diluted Liquid Phase. P123 triblock copolymers have a CMC (critical micelle concentration) in pure water of about 4.0×10^{-3}% (w/w) at 25 °C.[4] Above the CMC but at sufficiently low concentration, $d\Sigma/d\Omega$ was calculated assuming spherical, ellipsoidal (prolate and oblate), cylindrical shapes for the micelles.[23] It was found that SAXS intensities were best matched with the calculated values using a spherical form factor. Since the PPO blocks are more hydrophobic than the PEO, the micelles are made of a PPO core surrounded by a hydrated PEO shell. It has been shown that a core−shell model is therefore well adapted to describe these micelles.[24] At higher concentrations, interaction between P123 micelles takes place, and a peak arising from the structure factor, $S(q,R_{HS})$ where q is the wave vector transfer and R_{HS} is the hard sphere interaction radius, appears in the scattering intensity. There are different models, like Percus−Yevick (PY) and Rogers−Young (RY) closure with Ornstein−Zernike integration equation, to fit the structure factor for interacting hard spheres. These two models slightly differ from each other in the sense that the PY model is a little overestimating the main correlation peak compared to RY.[25] As this difference lies within the instrumental accuracy, the PY approximation was used in this analysis.[26] For an isotropic polydispersed solution of micelles, the scattered intensity can be calculated assuming some approximations according to two alternative models known as the DA (decoupling approximation) and LMA (local monodisperse approximation). In the DA, the scattered intensity in absolute units reads as

$$I(q) = r_e^2 n_p \langle P(q) \rangle S'(q, R_{HS}) \tag{1}$$

where $n_p = N_p/V$ is the number of micelles per unit volume, N_p is the total number of micelles, $\langle P(q, R) \rangle$ is the form factor of a micelle averaged over the distribution $f(R)$ of the micellar radii, $S'(q, R_{HS})$ is an effective structure factor, and $r_e = 2.85 \times 10^{-15}$ m is the classical radius of the electron. $S'(q, R_{HS})$ is related to the structure factor $S(q, R_{HS})$ by the following expression:[26]

$$S'(q, R_{HS}) = 1 + \beta(q, R_{HS})[S(q, R_{HS}) - 1] \tag{2}$$

where $\beta(q, R_{HS}) = |\langle P(q, R) \rangle|^2 / \langle |P(q, R)|^2 \rangle$.

The DA is valid for small volume fractions and low polydispersity where particles positions are independent of their size. Alternatively, one can consider that the positions are fully correlated to the size of the particles (where $\beta(q) = 1$) in the so-called "local monodisperse approximation" (LMA) and this approximation is more adapted to larger polydispersities even though no LMA or DA works at very large polydispersities. Both approximations are fully described in reference.[27]

In the simple core−shell model where the core and the shell have a uniform electron density, the form factor yields

$$P(q, R_C, R_S) = [(4\pi/3)(\rho_S - \rho_M)(R_C + R_S)^3 F(q, R_C + R_S) + (4\pi/3)(\rho_C - \rho_S) R_C^3 F(q, R_C)]^2 \tag{3}$$

where $F(q, R) = 3[(\sin qR - qR \cos qR)/(qR)^3]$ is the normalized amplitude scattered by a sphere, R_C and R_S are the radii of the core and the thickness of shell, and ρ_C, ρ_S, and ρ_M are the electron densities of the core, shell, and solvent. When mapping out the ternary phase diagram, the composition of the solvent that is a mixture of ethanol and water is changing. Its electron density ρ_M as to be calculated for each composition using following relation:

$$\rho_M = \frac{n_w Z_w + n_e Z_e}{V_M} N_A \tag{4}$$

where n_w and n_e are the number of moles of water and ethanol in the volume V_M of the solvent, $Z_w = 10$ and $Z_e = 26$ are the number of electrons in one mole of water and ethanol, and N_A is the Avogadro number.

More complex models in which a density profile of the shell[28] or the polymer conformation are taken into account are reviewed in the paper by Hamley et al.[29] In the following analysis, we have used the decoupling approximation[27] and local monodisperse approximations[26,27] in which we assumed a polydisperse core and a shell of constant thickness R_S. A Gaussian distribution was used to describe the polydispersity of the micelles radii. The Gaussian distribution is given by

$$f(R) = \exp\left[-\left(\frac{(R - \langle R \rangle)^2}{2\sigma^2}\right)\right] \tag{5}$$

where, $\langle R \rangle$ is the average radius of the micelles, σ is a root mean-square deviation from the mean radius and is related to the polydispersity δ by $\delta = \sigma/\langle R \rangle$. This model is well described by Pedersen[23] and was used for describing small angle scattering curves for micelles of block copolymers[29−32] and surfactant vesicles.[33] The detailed equations of this and Percus−Yevick structure factor are given in Supporting Information.

In the Percus−Yevick approximation, the volume fraction is one of the key parameters. It is therefore important to introduce this parameter in the calculation of the absolute intensity. This can be obtained by assuming that $\phi = N_p \langle V_{mic} \rangle / V = n_p \langle V_{mic} \rangle$. Under this approximation, the calculated intensity can be directly compared to the observed data measured in absolute intensity. For example, in the decoupling approximation this yields

$$I_{DA}(q) = \frac{r_e^2 \phi \langle P(q) \rangle S'(q, R_{HS})}{\langle V_{mic} \rangle} \tag{6}$$

This expression relies on the approximation that each micelle has the average volume, $\langle V_{mic} \rangle$ so that the total volume of the micelles is defined as $N_p \langle V_{mic} \rangle$.

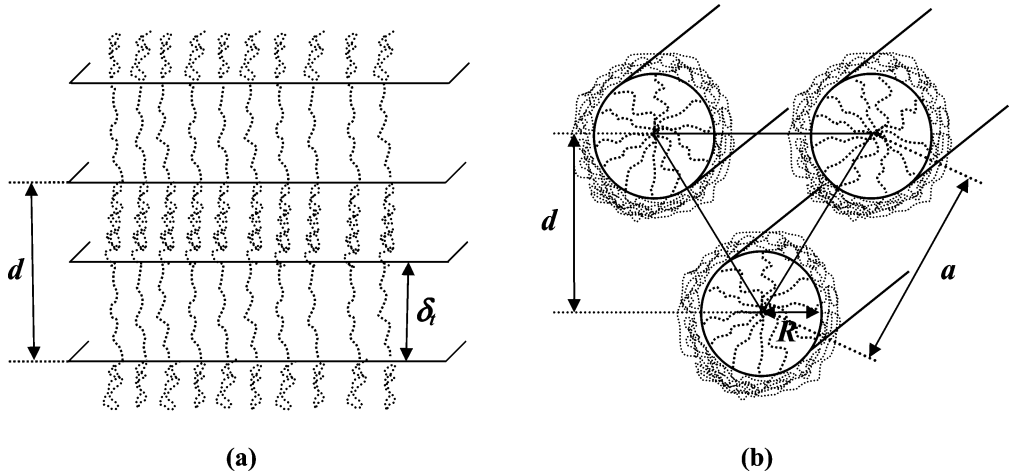

Figure 1. Schematics of (a) lamellar (L_α) and (b) hexagonal (H_1) crystalline phases with lattice parameter, d and/or a and thickness (δ_t) and radius (R) of apolar domain.

TABLE 1: Different Characteristics for Various Types of Lattices

lattice	N_{cell}	allowed reflections	positions of reflections	sequence of Bragg reflections	multiplicity m_{hkl}
FCC ($Fm3m$)	4	$f_{hkl} = 4$ for (h, k, l) even/odd	$q_{hkl} = \frac{2\pi\sqrt{(h^2+k^2+l^2)}}{a}$	$\sqrt{3}$:2:$\sqrt{8}$:$\sqrt{11}$:$\sqrt{12}$:4:$\sqrt{19}$:...	$m_{h00} = 6$ $m_{hh0} = 12$ $m_{hhh} = 8$ $m_{hk0} = 24$ $m_{hhk} = 24$ $m_{hkl} = 48$
hex ($P6mm$)	1	$f_{hkl} = 1$ for all reflections	$q_{hk} = \frac{4\pi\sqrt{(h^2+k^2+hk)}}{a\sqrt{3}}$	1:$\sqrt{3}$:2:$\sqrt{7}$:3:$\sqrt{12}$:$\sqrt{13}$:...	$m_{h0} = 6$ $m_{hh} = 6$ $m_{hk} = 12$
lam	1	$f_{hkl} = 1$ for all reflections	$q_h = \frac{2\pi h}{a}$	1:2:3:4:5:6:...	$m_h = 1$
HCPS ($P6_3mmc$)	2	$f_{hkl} = 2$ for ($h + 2k = 3n$) with l even $f_{hkl} = \sqrt{3}$ for ($h + 2k = 3n + 1$)U ($h + 2k = 3n + 2$) with l odd $f_{hkl} = 1$ for ($h + 2k = 3n + 1$)U ($h + 2k = 3n + 2$) with l even	$q_{hkl} = \frac{2\pi\sqrt{{}^4/_3(h^2+hk+k^2)+{}^3/_8 l^2}}{a}$	1:6/$\sqrt{32}$:$\sqrt{41/32}$:$\sqrt{68/32}$:$\sqrt{96/32}$:...	$m_{h00} = 6$ $m_{00l} = 2$ $m_{hh0} = 6$ $m_{hk0} = 12$ $m_{0kl} = 12$ $m_{hhl} = 12$ $m_{hkl} = 48$

For the local monodisperse approximations, the intensity reads as

$$I_{LMA}(q) = r_e^2 n_p S(q, R_{HS}) \int_{R_{c\,min}}^{R_{c\,max}} P(q, R_c) f(R_c)\, dR_c = r_e^2 \frac{\phi \langle P(q)\rangle S(q, R_{HS})}{\langle V_{mic}\rangle} \quad (7)$$

3.2. Crystalline Phases. For crystalline phases, correlations between the positions of micelles become strong enough to produce Bragg reflections. The width of the Bragg peaks is somehow inversely proportional to the size of the coherent scattering domains. The sequence of Bragg reflections defined by their Miller indices (hkl) is used to identify the nature of each phase. The intensity of the Bragg reflections is related to the multiplicity, m_{hkl}, of the reflections in the given space group. A Debye−Waller factor can be used to some extent to account for the effect of thermal fluctuations in the position of micelles. For lamellar phases, the width of Bragg peaks is affected on a more subtle way in the presence of thermal fluctuations because of the well-known Landau−Peierls instability associated to long-range loss of order.[34,35] For monodisperse micelles, the scattering cross-section is proportional to the product of the micellar form factor, $P(q)$ times the structure factor $m_{hkl}|F_{hkl}(q)|^2$ at a given reflection located at $q = G_{hkl}$ times the exponential Debye−Waller factor:

$$I(q) = \langle P(q)\rangle m_{hkl} |F_{hkl}(q)|^2 \exp[-q^2\sigma^2]\, \delta(q - G_{hkl}) \quad (8)$$

where G_{hkl} is a wave vector transfer corresponding to the particular hkl Bragg reflection. The calculated scattered intensity is obtained after convolution of the scattering intensity by the instrumental resolution function and by a Lorentzian function with a width equal to $2\pi/\xi$ related to the coherence length, ξ, of the scattering domains. The lorentz polarization factor is assumed to be 1 at such small angles.

3.2.1. Structural Parameters of the Lamellar and 2D Hexagonal Phases. The lattice parameters of the microstructure are the repeat distance, d (for lamellar structure), and the distance between the planes passing by two adjacent rows of cylinders, d (for the 2D hexagonal structure please see Figure 1). The position of the Bragg peaks in q space (the observed sequence of Bragg reflections) and their multiplicity for these two phases along with $Fm3m$ and $P6_3mmc$ are given in Table 1. The position of the first Bragg reflection, q_1 (equal to q_{10} for the

2D hexagonal phase), is used to compare the lattice parameters of these two phases in the following way:

$$d = \frac{2\pi}{q_1} \quad \text{(lamellar)}; \qquad d = \frac{2\pi}{q_{10}} = \frac{\sqrt{3}}{2}a \quad \text{(hexagonal)} \quad (9)$$

The thickness of the apolar domain (PPO and some ethanol), δ_t (for lamellar structure), and the radius of the apolar domain R (for hexagonal structure) are given by

$$\delta_t = df \quad \text{(lamellar)}; \qquad R = a\left(\frac{\sqrt{3}f}{2\pi}\right)^{1/2} \quad \text{(hexagonal)} \quad (10)$$

in which f is the apolar volume fraction which is calculated by using the following equation,[36]

$$f = 0.73\phi_P + x\phi_S \quad (11)$$

where 0.73 corresponds to the volume fraction of the PPO block in P123 and ϕ_p and ϕ_S are the volume fraction of copolymer and solvent, respectively, in the ternary system, and x denotes the fraction of the solvent, which is located in the PPO rich domains. To convert the weight fraction of the components into volume fractions, the bulk densities of the P123 copolymer (1.018 g/cm^3), water (0.998 g/cm^3), and ethanol (0.788 g/cm^3) are used.[37]

The interfacial area, a_p which is the area that one PEO block occupies at the polar and apolar interface, is determined from

$$a_P = \frac{v_P f}{2\delta_t \phi_P} \quad \text{(lamellar)}; \qquad a_P = \frac{v_P f}{R\phi_P} \quad \text{(hexagonal)} \quad (12)$$

where v_P is the volume of one PPO copolymer molecule. For P123, v_P is equal to 9.2963 nm^3.

3.2.2. Intermediate Phase (Mixture of Cubic and HCPS). In addition to the lamellar, 2D-hexagonal, and liquid isotropic phases, we found an intermediate phase composed of a mixture of cubic *Fm*3*m* and *P*6$_3$*mmc* (hexagonally close packing of spheres (HCPS)) phases. This was observed around 30% (w/w) of P123 and below 5% (w/w) ethanol. At 10% (w/w) ethanol, the HCPS phase only remained.

The assignment of the crystallographic space group of the cubic liquid crystalline phases is more difficult than for the 2D hexagonal and lamellar structures. The correct indexing of the cubic structure to a crystallographic space group is often difficult because of the small number of reflections and their relatively low intensities. It is necessary to consider not only the relative positions of the diffraction peaks but also their relative intensities as well as other criteria like the missing peaks, the values of the lattice parameter, and the interfacial area per PEO block. The indexing of the SAXS diffraction peaks to a crystallographic group was assessed by plotting the reciprocal spacing, $1/d_{hkl}$, of the reflections versus the sum of the Miller indices, $(h^2 + k^2 + l^2)^{1/2}$. This curve should be a line passing through the origin of the graph with a slope of $1/a$, where a is the corresponding cubic cell lattice parameter.[38−40]

The characteristics sequence of Braggs reflections with their multiplicity are listed in Table 1 for the *Fm*3*m* and *P*6$_3$*mmc* (HCPS) crystalline phases. For HCPS, the relation between the two unit cell dimensions of the hexagonal Bravais lattice is $c = (8/3)^{1/2}a$.

3.3. Programming. In the isotropic phase, a MATLAB program has been developed to fit on an absolute scale the observed data to the above description. Eight parameters could be either fixed or adjusted, among which five describe the form factor, one for the polydispersity of the micelle core radius, and two for the structure factor (depending on the model). These parameters are namely R_C and R_S (the radii of the core and thickness of shell), ρ_C and ρ_S (their corresponding electron densities), δ (the polydispersity), volume fraction, ϕ, and hard sphere interaction radius R_{HS} of micelles. In the crystalline phases, the program was used to identify the peak positions.

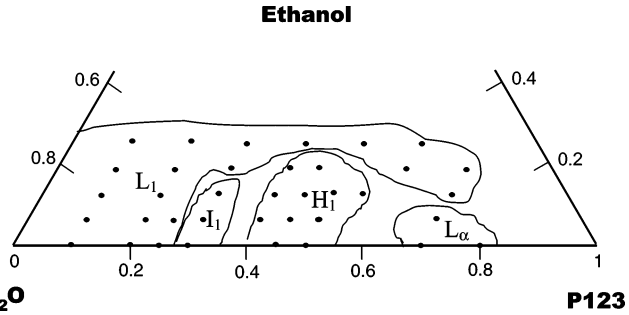

Figure 2. Ternary phase diagram of P123/water/ethanol at $T = 23$ °C. L_1 denotes region with isotropic solution (water rich), I_1 denotes the clear isotropic gels and mixture of cubic and HCPS lattice, H_1 denotes cylindrical micelles arranged in a 2D hexagonal lattice, and L_α denotes the lamellae−planner micelles. The boundaries of the one−phase regions are drawn with solid lines. Points indicate the compositions of P123/water/ethanol in ternary mixture.

3.4. Optical Mapping of the Phase Diagram. It is important to note that the existence of the different phases can be estimated by simple optical observation. Such an observation is also useful to estimate whether a phase separation occurs in the sample cell. When this is the case at the macroscopic level, two distinct phases are optically visible and separated by a clear boundary. On the contrary, homogeneous phases lead to homogeneous and transparent media.

All samples have been checked optically between crossed polarizer and analyzer. Lamellar and 2D hexagonal phases are birefringent, whereas cubic with HCPS and diluted isotropic phases are not. Cubic and hexagonal phases are gels, whereas the lamellar phase is fluid in our case. The fluid versus gel aspect simply means here that some solutions flow while others do not when the vials are rotated. The phase diagram obtained from optical observations and prior to the SAXS experiments analysis is shown in Figure 2.

4. Results and Discussion

The liquid L_1, intermediate (mixture of cubic and HCPS) I_1, hexagonal H_1, and lamellar L_α phases were clearly identified by SAXS, in the corresponding locations ascertained by the optical observations. Such phases (except the mixture of cubic and HCPS) were already observed in different cosolvents (such as formamide, propylene glycol, xylene, etc.).[41−48] In the following, the different scattering curves and their analysis are discussed phase by phase with the aim to evidence the role of three components on the morphology of the scattering objects.

4.1. Liquid Phase. *4.1.1. The Binary System: P123 Block Copolymer in Pure Water.* The SAXS curves measured for the binary P123/water system are shown in Figure 3 for two P123 concentrations 10 and 20% (w/w). At 10% (w/w) of P123, the correlation between micelles is weak, while at 20% (w/w) a peak emerges in the low q region of the scattering curve indicating that the micelles are correlated in position.

We have fitted the SAXS curves using the DA and LMA models described in the theoretical section. We found that both models yield very good fits and are hardly distinguishable. For sake of simplicity, we restrict the discussion to the parameters

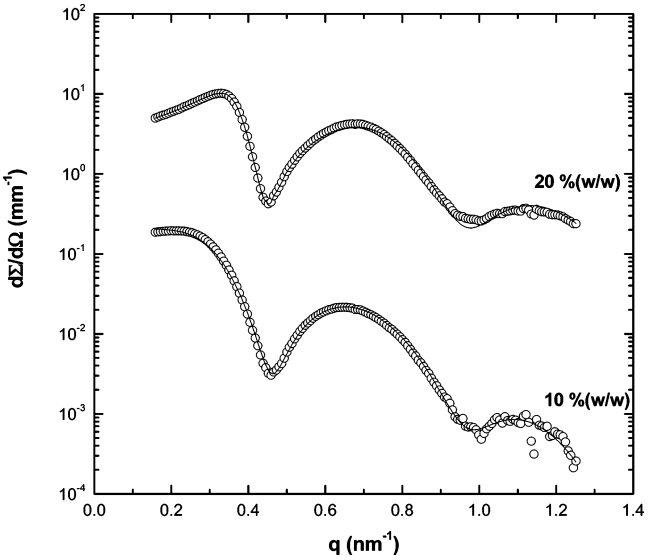

Figure 3. SAXS curves in liquid phase of the P123/water. The lines indicate fitting using the core−shell model. Solid line corresponds to calculated intensity using local monodisperse approximation. Curves are shifted for clarity with multiplication factor 5.

obtained from the LMA model only. The fitted curves with the parameters from the DA model are given in the Supporting Information. The fitting parameters are reported in Table 2 with error bars indicating the range over which no significant changes could be detected in the adjustment.

In the fits, the solvent (i.e., water or water + ethanol) electron density was kept fixed to the calculated value obtained from eq 4 (see column 3 of Table 2) while the core and shell electron densities were considered as free parameters. As a guideline, the electron densities of pure PPO and PEO blocks in the melt were calculated. We obtained 338.2 e^-/nm^3 and 334.4 e^-/nm^3, respectively, by assuming that each of the two materials had a mass density of 1.018 $g\cdot cm^{-3}$ equal to the mass density of the P123 block copolymer. The water electron density was fixed to 334.5 e^-/nm^3. This value is incidentally very close to the one calculated for the PEO block in the melt. This means that the PEO block would be indistinguishable from water if it were to behave as in the melt.

At 10 and 20% (w/w) of P123 in water, the fitted core and shell electron densities were ∼337 e^-/nm^3 and ∼329 e^-/nm^3, respectively. The fitted PPO electron density is thus quite close to the value calculated for the melt, that is, 337.5 e^-/nm^3. This is not the case for the fitted PEO electron density which is found to be ∼329 e^-/nm^3 and has to be compared to the value calculated for the melt: 334.4 e^-/nm^3. This shows that it is not possible to fit the data with a pure PEO shell with PEO melt density, and PEO chains are expected to be solvated by water. The lower electron density of the PEO water shell is somewhat surprising since the electron density of water is similar to the one of melt PEO. If we assume that the PEO and water shell give a homogeneous medium characterized by a single electron density (ρ_S in Table 2), a possible explanation is that either the water molecules or the PEO blocks or both at the same time slightly expand in volume by 1.66% when mixed. This assumption is somehow disputable, and it is expected that the concentration of PEO blocks depends on the distance to the PPO core interface.

When we compare the radii of micelles prepared in aqueous mixtures with 10 and 20% (w/w) of P123, we observed that the radius of the core of the micelles, R_C, increased from 4.3 to 4.6 nm while the shell radius, R_S, decreased from 3.7 to 3.3 nm. This is showing that the diminution of the water amount reduces the swelling of the PEO blocks in the shell. The hard sphere interaction radius was found to decrease from 9.2 to 8.9 nm upon increasing the P123 concentration. Therefore, the larger the concentration of P123, the smaller the intermicellar distance.

The R_{HS} values that we have found are bigger than the ones reported by Ganguly et al.[21] with a larger core (R_C = 6.4 nm) compared to our result. This is evidencing that the two experiments do not have the same sensitivity to the shell thickness. In neutron experiments (SANS experiments[21]) there is a stronger contrast between the copolymer blocks and the heavy water (D_2O) but not sufficiently high between the two polymer materials in order to distinguish one from the other.

The electron density of the PPO blocks is found close to the one of the melt, so that it is reasonable to assume that the core is made of PPO blocks only. The so-called aggregation number, N_{agg}, defined as the number of P123 molecules per micelle is given either by

$$N_{agg} = (4\pi R_C^3)/(3n_{PO}V_{PO}) \quad (13)$$

or alternatively by

$$N_{agg} = (4\pi R_{HS}^3/3)C/\phi \quad (14)$$

where V_{PO} is the volume of one PPO monomer, n_{PO} is the number of these monomers per block (here n_{PO} = 70), $C = cN_A/1000$ where c is the concentration (in mol/cm^3) of the P123 in the system considering all the polymers molecules participating to the aggregates (CMC ∼4×10^{-3}% (w/w)), R_{HS} is the hard sphere radius, N_A is the Avogadro number, and ϕ is the micellar volume fraction. When using eq 13, N_{agg} is directly related to the core radius R_C, that is to say, to the form factor

TABLE 2: Electron Density of Solvents (ρ_M), Core Radius (R_C), Electron Density of Core (ρ_C), Thickness of the Shell (R_S), Micellar Radius (R_m), Electron Density of Shell (ρ_S), Polydispersity (δ), Hard Sphere Interaction Radius (R_{HS}), Volume Fraction (ϕ) and Aggregation Number (N_{agg}) for Copolymer Solutions at 23 °C

			parameters of $F(q)$					parameters of $S(q)$		calculated parameters		
polymer concn %(w/w)	ethanol concn %(w/w)	ρ_M[a] (e^-/nm^3)	R_C nm ± 0.1	ρ_C (e^-/nm^3)	R_S nm ± 0.1	ρ_S (e^-/nm^3)	δ ± 0.01	R_{HS} nm ± 0.1	ϕ ± 0.01	R_m nm ± 0.1	N_{agg} eq 13 ± 2	N_{agg} eq 14 ± 2
10	0	334.5	4.3	336.8	3.7	328.2	0.15	9.2	0.17	8.0	50	199
20	0	334.5	4.6	337.2	3.3	329.2	0.13	8.9	0.28	7.9	62	220
	5	328.6	4.2	332.1	3.1	324.6	0.14	8.3	0.30	7.3	47	169
	10	323.7	3.7	324.3	3.2	318.3	0.16	7.7	0.31	6.9	32	133
	15	318.9	3.4	318.5	3.2	314.3	0.21	7.5	0.33	6.6	25	112
	20	314.3	2.9	313.3	3.3	310.5	0.25	6.7	0.34	6.2	15	73

[a] ρ_M is the fixed parameter during the fitting, and it is calculated from eq 4.

of the micelles. Conversely in eq 14, N_{agg} is also related to the volume fraction ϕ and R_{HS}, in other words to the structure factor. The two calculated values of N_{agg}, reported in the last two columns of Table 2, are somewhat different; the one obtained from the hard sphere structure factor (eq 14) is much higher than the one obtained from the form factor (eq 13). As a matter of fact, both values show the same trend upon water dilution and/or addition of ethanol as discussed later on. We believe that this difference comes from the fact that the R_{HS} used in eq 14 for calculating the N_{agg} includes a lot of solvent molecules and therefore overestimates the number of polymer molecules in this volume giving a higher N_{agg} value. Bearing in mind that the micelle−micelle interaction might be more subtle than just hard sphere interactions, we considered in the following that the N_{agg} derived from eq 13 are more reliable. This is also supported by the fact that our fitting model shows a higher sensitivity to the parameters entering in the form factor calculation (such as the core radius) than to the parameters entering in the structure factor calculation. As expected for block copolymers, N_{agg} and the volume fraction ϕ increases with increasing concentration of P123 from 10 to 20% (w/w), meaning that micelles are composed of more and more copolymer molecules.

The surface area of the core of each micelle, S_C, can be also calculated from the radius of the core: $S_C = 4\pi R_C^2$. This in turn allows one to deduce the surface occupied per PPO block at the interface with the PEO blocks from S_C/N_{agg}. This gives $S_{PPO} = 4.65$ and 4.29 nm^2 at 10 and 20% (w/w) P123 concentrations, respectively, meaning that the surface per PEO molecule at the PPO interface evolves from $S_{PEO} = 2.32$ to 2.14 nm^2 when increasing the P123 concentration. If now we use the aggregation number obtained from the structure factor (last column of Table 2) instead of the one obtained from the form factor, these surface areas scale with the ratio of these two aggregation numbers: $S_{PPO} = 1.16$ and 1.21 nm^2 at 10 and 20% (w/w) P123 concentrations, respectively. Note that all these values are comparable to the ones obtained for P105 (PEO_{26}-$PPO_{40}PEO_{26}$) and P85 ($PEO_{37}PPO_{58}PEO_{37}$) from Aramaki et al.[49] In the following, as explained just before, we will consider the values calculated from the aggregation number obtained from the form factor. Thus, when the concentration of P123 increases, the surface per PPO−PEO junction at the core/shell interface (S_{PPO}) decreases slightly, the shell layer thickness decreases, and the electron density remains constant. This could point toward a loss of water molecules in the shell layer that cannot be addressed unambiguously from our fits since the water molecules and PEO blocks appear with nearly the same contrast with X-rays.

4.1.2. Block Copolymer in Water/Ethanol Mixture. Unlike water, which is a PEO block selective solvent, ethanol is known to be a good solvent for both the PEO and PPO blocks. The addition of ethanol thus has a significant influence on the self-assembly behavior of these block copolymers in aqueous medium. Increasing the ethanol concentration of the aqueous copolymer solution yields an increase of the CMT (critical micelle temperature) and CMC and a decrease of the aggregation number of the copolymer micelles.[50] Figure 4 shows several SAXS curves measured for solutions at constant composition of P123 (20% (w/w)) as a function of the water/ethanol ratio. These scattering curves show that when the concentration of ethanol becomes higher, the correlation peak found around 0.3 nm^{-1} shifts toward higher q wave vector transfers values, while the amplitude of the second peak, related to the form factor of the micelles, decreases. This is a clear indication of the important

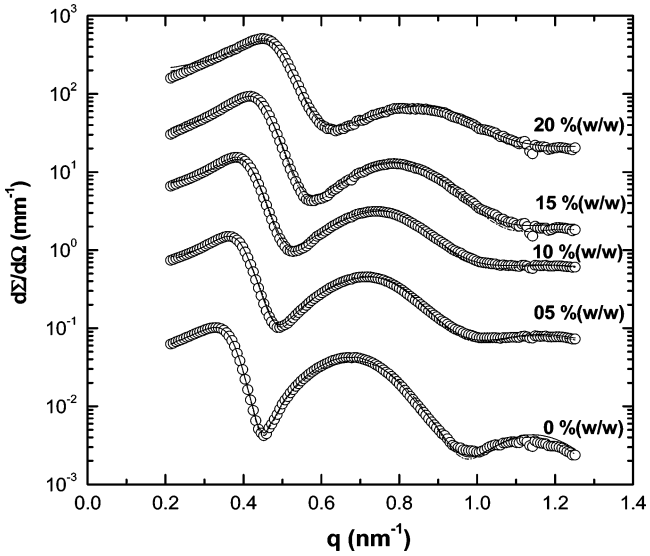

Figure 4. SAXS curves for effect of ethanol on 20% (w/w) of P123. The concentration of ethanol varies from 0 to 20% (w/w). The solid line indicates the fit using local monodisperse approximation. Curves are shifted for clarity with multiplication factor 5.

role played by ethanol on the interaction between micelles and on their morphology. The parameters obtained from the fits are depicted in Table 2. For all fits, the solvent (water + ethanol) electron density was calculated and then fixed to its nominal value according to its composition. Analysis of the data shows that the micellar radius, the core size, and subsequently the aggregation number of the micelles steadily decrease when the concentration of ethanol increases. The shell thickness stays almost constant. In addition, the volume fraction ϕ obtained from the structure factor adjustment slightly increases when the amount of ethanol increases. The concomitant decrease of the aggregation number and of the radius of the core is consistent with the decrease of the micellar volume.

One can thus conclude that ethanol favors the apparition of smaller micelles but with a higher number density, so that overall, the volume fraction of all the hard spheres increases. This is reflected in the value of R_{HS} (column 9 of Table 2) and in Figure 4 by a shift of the correlation peak positions to higher q values indicating that the mean intermicellar distance decreases upon addition of ethanol. The decrease of the second peak intensity (from the form factor) is attributed to a lower contrast of the shell electron density with the solvent when ethanol is added or, alternatively, to the possible increase in the polydispersity of the spherical micelles. The small micelles with a large part of the surfactant hydrophobic chains in contact with the solvent are unfavorable in pure water because the interfacial tension between water and hydrophobic PPO chains is high. The addition of ethanol to water reduces the interfacial tension between the hydrophobic chains and the solvents so that the formation of smaller micelles becomes more favorable.

We were not able to fit the scattering curves when the electron density of the PPO core was fixed to the one found with pure water dilution (337 e$^-$/nm^3). A clear decrease of this parameter was observed upon the addition of ethanol (see columns 5 of Table 2). This means either that ethanol diffuses inside the core or that the PPO density per block decreases in a PPO melt. The mixing of ethanol and PPO in the core is more probable since ethanol is known to be a good solvent for both PEO and PPO. In the hypothesis that PPO blocks and ethanol molecules do not change in mean volume when mixing, we can infer a fraction

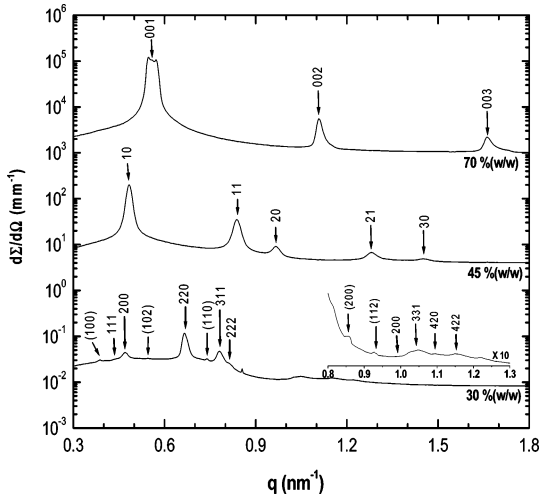

Figure 5. Diffraction pattern of cubic + HCPS phases (30% (w/w)), 2D hexagonal (45% (w/w)) and lamellar (70% (w/w)). For 30% (w/w) P123, the indexing of peaks are indicated without brackets (for *Fm*3*m*) and with brackets (for HCPS). The first-order lamellar peak (upper curve) is not a double peak but it is a detector saturation problem. The inset of the bottom curve shows partial magnification. Curves are shifted for clarity with multiplication factor 5.

of ethanol in the core from the fitted electron density values ρ_c by using the following equation:

$$\rho_c = \phi_e \rho_e + (1 - \phi_e)\, \rho_{PPO} \qquad (15)$$

where, ϕ_e, ρ_e, and ρ_{PPO} are, respectively, the volume fraction of ethanol in the core, the electron density of ethanol (273.2 e^-/nm^3), and the bulk electron density of PPO in core (338.2 e^-/nm^3). This yielded $\phi_e = 12$, 27, 40, and 60% present in the core at 5, 10, 15, and 20% (w/w) of ethanol composition, respectively. With ethanol present in the core, the core radius and the aggregation number decrease and the micellization becomes less favorable since a better solvent environment for both PEO and PPO blocks of copolymer occurs. The values of ethanol fraction present inside the micellar core will be used later in the calculation of the volume fraction of the PPO domains *f* (see eq 11) in the crystalline phase.

4.2. Crystalline Phases. *4.2.1. Overview of the Liquid Crystalline Phases in the Water/P123 Binary System.* For the binary system water/P123, crystalline phases were obtained in the concentration range 30% (w/w) to 80% (w/w) which was the highest prepared concentration. The phase identification was made through the sequence of Bragg peaks that were observed. Figure 5 shows typical diffraction patterns observed in this concentration range. These patterns are respectively consistent with a mixture of a cubic and a HCPS, a pure 2D hexagonal, and a pure lamellar phase.

4.2.2. Lamellar (L_α) and Hexagonal (H_1) Liquid Crystalline Phases. Microstructures consisting of planar and cylindrical micelles were present in the lamellar and hexagonal crystalline region, respectively, shown in Figure 2. Typical SAXS diffraction patterns obtained at 70% (w/w) (lamellar) and 45% (w/w) (2D-hexagonal) of P123 are shown in Figure 5. The lattice parameter *d*, the volume fraction of the apolar domain *f*, the thickness of the apolar layer δ_t (for L_α phase) or the radius of the apolar cylindrical micelle *R* (for H_1 phase), and the interfacial area of PEO block a_p are summarized in Table 3 for all samples.

In this binary part of the phase diagram, the lattice parameter decreases when increasing the copolymer concentration throughout the whole phase diagram. This is a consequence of a higher packing of the copolymer molecules. Alternatively, a reduction of the curvature of the interfaces or simply the reduction of the water swelling of PEO blocks surrounding PPO layers (for lamellar phase) or cylinders (for hexagonal phase) would produce the same effect. Information on the packing of the aggregates is also given by the interfacial area per PEO block, a_p. The determination of this parameter provides valuable understanding of the ethanol effect at the molecular level. The interfacial area can be related to the lattice parameter through simple geometrical considerations. For the binary copolymer−water system, we assume that there is no water present in the PPO apolar domain (i.e., $f = 0.73\phi_p$ in eq 11). The last column of Table 3 shows a decrease in the interfacial area with increase in copolymer concentration, this in the absence of ethanol or at a fixed ethanol content (in this latter case water molecules are replaced by copolymer molecules). This decrease of "*d*" takes place since the packing of the PEO blocks increases (i.e., decrease in area per PEO block, a_p), while the water content and water availability decreases (osmotic effect). However, the variations of the interfacial area within each liquid crystalline microstructure are small. For the binary copolymer−water system, the assumption made in the calculation of a_p are correct, that is, only the PPO block participates in the apolar volume fraction. As expected, water is a solvent selective for the PEO blocks of the copolymer but not for the PPO blocks.

Influence of Ethanol. At a given copolymer concentration, the same decreasing trend in the lattice parameter *d* was

TABLE 3: Structural Parameters for Lamellar (L_α) and Hexagonal (H_1) Crystalline Phases Calculated from the Lattice Parameter *d* and Absolute Volume Fractions *f* at 23 °C

phase	volume fraction ϕ_P	volume fraction ϕ_{water}	volume fraction $\phi_{ethanol}$	volume fraction of apolar domain *f*	lattice parameter *d* (nm)	thickness of apolar domain[a] δ_t (nm)	radius of apolar domain[a] *R* (nm)	interfacial area a_p (nm^2)
L_α	0.70	0.30	0	0.51	11.42	5.82		1.16
	0.80	0.25	0	0.58	10.30	5.97		1.13
	0.70	0.19	0.06	0.55	10.65	5.86		1.25
H_1	0.45	0.55	0	0.33	14.99		5.22	1.32
	0.49	0.51	0	0.36	14.51		5.27	1.30
	0.39	0.55	0.06	0.36	14.66		5.33	1.62
	0.39	0.49	0.12	0.45	13.98		5.69	1.85
	0.39	0.44	0.17	0.53	13.19		5.82	2.18
	0.45	0.49	0.06	0.40	14.28		5.48	1.52
	0.45	0.43	0.12	0.48	13.41		5.63	1.76
	0.45	0.38	0.17	0.55	12.51		5.63	2.02
	0.49	0.45	0.06	0.42	13.95		5.48	1.46
	0.49	0.39	0.12	0.50	13.12		5.62	1.70
	0.53	0.35	0.12	0.51	12.96		5.61	1.60

[a] Parameters are calculated from the experimentally derived lattice parameter *d*.

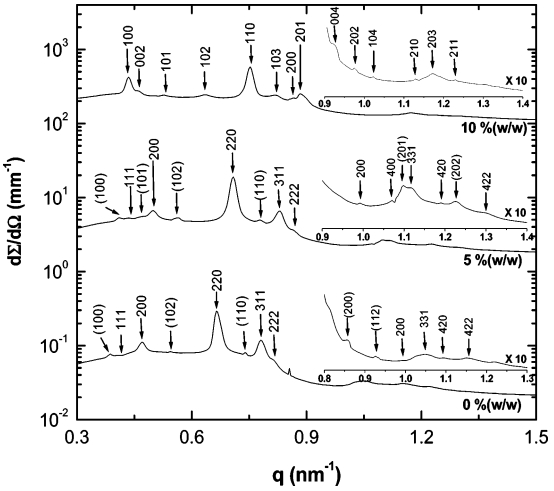

Figure 6. Diffraction pattern showing the effect of ethanol on 30% (w/w) P123. For 0 and 5% (w/w) ethanol, the indexing of peaks are indicated without brackets (for *Fm*3*m*) and with brackets (for HCPS). For 10% (w/w) ethanol, the phase indexes are from HCPS only. Curves are shifted for clarity with multiplication factor 5. The inset of each curve shows partial magnification.

TABLE 4: Structural Parameters in the Intermediate, (I_1) (Cubic and HCPS) Crystalline Phases

	volume fraction			apolar volume fraction	lattice parameters (nm)		
					*Fm*3*m*	*P*6$_3$*mmc*	
phase	ϕ_P	ϕ_{water}	$\phi_{ethanol}$	*f*	*a*	*a*	*c*
*Fm*3*m*	0.30	0.70	0	0.21	25.73	19.20	31.35
+ *P*6$_3$*mmc*	0.30	0.64	0.06	0.30	24.32	18.50	30.21
*P*6$_3$*mmc*	0.30	0.59	0.11	0.41		16.75	25.30

observed by replacing water with ethanol. This reduction of *d* is accompanied by the mixing of ethanol in core and shell which leads to an increase in volume fraction of apolar domain (rich in PPO) and to a decrease in water hydration of PEO blocks (PEO rich domain contains less solvent and less water molecules per PEO block). Without a precise measurement of the aggregate form factor (membranes and cylinders scattering), it is impossible to address precisely the evolution in thickness of the PPO and PEO rich domains. Moreover, it is reported[40] that even in the PEO−PPO−PEO/water binary system ideal linear swelling laws are not observed as seen for low molecular weight surfactants.[51,52] The tendency of decrease in the lattice parameter with increasing ethanol content is observed in all liquid crystalline phases measured here and at all copolymer concentrations.

If ethanol is present in the PPO core, this has to be taken into account to obtain the interfacial area (using eq 12). To calculate the volume fraction of apolar domains, *f*, in the crystalline phase, we have considered that the amount of ethanol present in the core would be the same as the amount observed in the micellar solutions at similar ethanol/water fractions. When the ethanol volume fraction is increased the interfacial area a_p becomes larger since apolar volume fraction increase. This calculation based on the measured *d* spacing indicates that the introduction of ethanol counterbalances the deswelling of the PEO blocks upon the decrease of the water content in the solvent mixture and even further increases the interfacial area by swelling both PEO and PPO blocks. Therefore, these calculations based on the presence of ethanol in the PPO block apolar domain are supported by the *d* measurements. A similar effect on lattice parameter and interfacial area for PEO−PPO−PEO block copolymers is observed in a ternary system with water and butanol.[47]

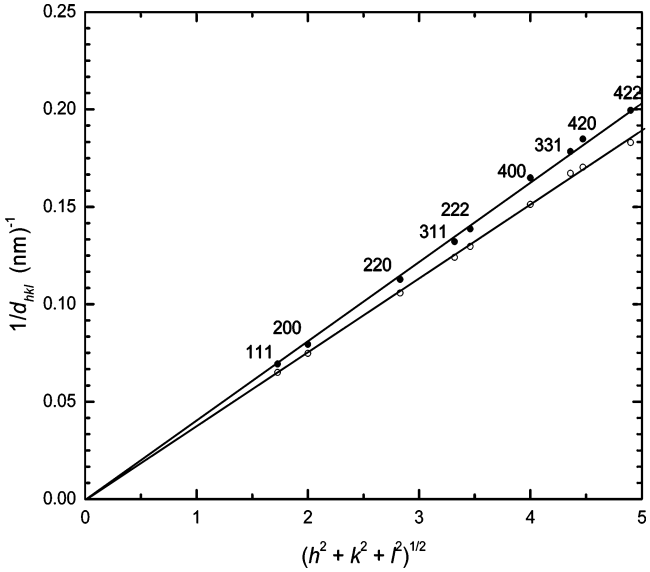

Figure 7. Plots of the $1/d_{hkl}$ versus $(h^2 + k^2 + l^2)^{1/2}$ for SAXS spectra of I_1 (cubic phase) (30% (w/w) P123 in the presence of ethanol): (○) 0% (w/w), (●) 5% (w/w) of ethanol. The Millar indices of *Fm*3*m* crystalline phase are indexed and are denoted in the graphs.

These explanations are supported by the calculations of the radius of apolar domains and apolar layer thickness obtained from eq 10. In the absence of ethanol, the apolar domains increase in size as the copolymer volume fraction increases assuming that no water enters the PPO core in the absence of ethanol. This increase is obvious because the increase of the copolymer content makes a substitution of water, which leads to an increase of the polar domain. The addition of ethanol leads to the increase of the apolar domain since ethanol enters PEO and PPO blocks.

4.2.3. Intermediate Phase (Cubic and HCPS Liquid Crystalline Phases). Around 30% (w/w) of P123, we have observed an intermediate phase located between the 2D hex and the isotropic phases. Since in this region the solvent content is higher than in the 2D hex phase, one can infer that the curvature of this phase should be more pronounced than in the 2D hex phase. This suggests that the micelles are spherical and close packed. Possible crystalline structures with spherical micelles are the bcc (*Im*3*m*) or the *Pm*3*n* cubic structures. However a close look to the scattering patterns presented in Figure 6 shows that the Bragg peak positions and intensities are not consistent with such symmetries. Seven to eight Bragg peaks with higher order peaks having very low intensities are observed. In addition, the first Bragg peak is very weak which is not expected from simple primitive or body centered cubic lattices.

As depicted in Figure 6, some of the Bragg reflections can be indexed in the *Fm*3*m* crystalline space group for 0 and 5% (w/w) ethanol while the remaining peaks are obeying the sequence observed for hexagonally close packed spheres (HCPS). We thus consider that we have a mixture of *Fm*3*m* and HCPS crystalline phases for 0 and 5% (w/w) ethanol in 30% (w/w) P123. As far as we know, this was not yet reported in the ternary phase diagram for PEO−PPO−PEO type block copolymer. The refinement of the peak positions for both structures allowed us to extract the lattice parameters of each phase. In the cubic phase, the lattice parameter (reported in Table 4) was obeying the usual linear behavior when plotting $1/d_{hkl}$ versus $(h^2 + k^2 + l^2)^{1/2}$ (see Figure 7). In the HCPS, the lattice

parameter c was calculated by using the relation $c = (8/3)^{1/2}a$. For 10% (w/w) ethanol in 30% (w/w) P123, we have observed that only one phase remains with a sequence of Bragg reflections consistent with the HCPS space groups.

Conclusion

The ternary phase diagram of the P123 block copolymer mixed with water and ethanol, for ethanol mass fractions less than 25%, was constructed by SAXS. Along the binary axis (P123/water), the following sequence of phases, $L_\alpha \rightarrow H_1 \rightarrow I_1$ (mixture of $Fm3m$ and $P6_3mmc$ phases) $\rightarrow L_1$, is observed when the copolymer concentration decreases. This sequence is preserved at low ethanol concentration. The isotropic phase is well described by interacting spherical micelles modeled within the framework of the Percus−Yevick approximation. In the model, the spherical micelles have a polydisperse core and a uniform shell of constant thickness. The fit to the data provided information about the evolution of the micelle form when changing relative volume fractions of the mixture. In particular, by fitting the electron densities, the radius of the core, and the thickness of the shell, we observed that the micelles became smaller as the ethanol concentration was increased. This effect is due to the reduction of the aggregation number caused by the presence of ethanol inside the core of the micelles and is concomitant with the increase in volume fraction. For higher polymer concentration phases, the fractioning of ethanol in the PPO and PEO domain are also supported by the evolution of the mean distance d between aggregates (membrane or cylinders). The precise thickness evolution of apolar and polar domains was not possible since we could not extract the aggregates form factors from our scattering curves. By increasing the concentration of P123 we also observed the appearance of cubic, 3D hex, 2D hex, and lamellar phases. In the region close to 30% (w/w) of P123, a cubic phase having the $Fm3m$ crystallographic symmetry coexists with a HCPS crystalline phase. This occurs for 0 and 5% (w/w) ethanol whereas for 10% (w/w) of ethanol only the 3D hex phase exists.

Acknowledgment. The authors are greatly indebted to the European Synchrotron Radiation Facility (ESRF) for the use of the ID02 beam line.

Supporting Information Available: The detailed equations for PY structure factor and the fitted curves with the parameters from the DA model are given in the Supporting Information. The fitting parameters are also reported in the table.

References and Notes

(1) Alexandridis, P.; Spontak, R. J. *Curr. Opin. Colloid Interface Sci.* **1999**, *4*, 130.
(2) Hamley, I. W. *Developments in Block Copolymer Science and Technology*; Hamley, I. W., Ed.; John Wiley & Sons, Ltd.: Chichester, U.K., 2004.
(3) Glatter, O.; Scherf, G.; Schiller, K.; Brown, W. *Macromolecules* **1994**, *27*, 6046.
(4) Wanka, G.; Hoffmann, H.; Ulbricht, W. *Macromolecules* **1994**, *27*, 4145.
(5) Hamley, I. W.; Mortensen, K.; Yu, G. E.; Booth, C. *Macromolecules* **1998**, *31*, 6958.
(6) Alexandridis, P.; Zhou, D.; Khan, A. *Langmuir* **1996**, *12*, 2690.
(7) Mortensen, K. *Macromolecules* **1997**, *30*, 503.
(8) Svensson, B.; Alexandridis, P.; Olsson, U. *J. Phys. Chem. B* **1998**, *102*, 7541.
(9) Holmqvist, P.; Alexandridis, P.; Lindman, B. *J. Phys. Chem. B* **1998**, *102*, 1149.
(10) Mortensen, K.; Brown, W. *Macromolecules* 1993, *26*, 4128.
(11) Alexandridis, P. *Curr. Opin. Colloid Interface Sci.* **1997**, *2*, 478.
(12) Caragheorgheopol, A.; Schlick, S. *Macromolecules* **1998**, *31*, 7736.
(13) Zhou, S. Q.; Su, J.; Chu, B. *J. Polym. Sci. B: Polym. Phys.* **1998**, *36*, 889.
(14) Kresge, C. T.; Leonowicz, M. E.; Roth, W. J.; Vartuli, J. C.; Beck, J. S. *Nature* **1992**, *359* (6397), 710.
(15) Brinker, C. J.; Lu, Y. F.; Sellinger, A.; Fan, H. Y. *Adv. Mater.* **1999**, *11*, 579.
(16) Zhao, D.; Huo, Q.; Feng, J.; Schmelka, B. F.; Stucky, G. D. *J. Am. Chem. Soc.* **1998**, *120*, 6024.
(17) Gibaud, A.; Grosso, D.; Smarsly, B.; Baptiste, A.; Bardeau, J. F.; Babonneau, F.; Doshi, D. A.; Chen, Z.; Brinker, C. J.; Sanchez, C. *J. Phys. Chem. B* **2003**, *107*, 6114.
(18) Gibaud, A.; Baptiste, A.; Doshi, D. A.; Brinker, C. J.; Yang, L.; Ocko, B. *Euro. Phys. Lett.* **2003**, *63*, 833.
(19) Gibaud, A.; Doshi, D. A.; Ocko, B.; Goletto, V.; Brinker, C. J. *Studies in Surface Science and Catalysis*; Park, S.-E. et al., Eds.; Elsevier: Amsterdam, The Netherlands, 2003; Vol. 146, p 351.
(20) Doshi, D. A.; Gibaud, A.; Goletto, V.; Lu, M.; Gerung, H.; Ocko, B.; Hang, S.; Brinker, C. J. *J. Am. Chem. Soc.* **2003**, *125*, 11646.
(21) Ganguly, R.; Aswal, V. K.; Hassan, P. A.; Gopalakrishnan, I. K.; Yakhmi, J. V. *J. Phys. Chem. B* **2005**, *109*, 5653.
(22) Narayan, T.; Diat, O.; Boesecke, P. *Phys. Rev. A* **2001**, *467−468*, 1005.
(23) Pedersen, J. S. *Adv. Coll. Interface Sci.* **1997**, *70*, 171.
(24) Zhang, K.; Khan, A. *Macromolecules* **1995**, *28*, 3807.
(25) Klein, R.; D'Aguanno, B. *Light Scattering: Principles and Development*; Brown, W., Ed.; Clarendon Press: Oxford, 1996, 30.
(26) Percus, J. K.; Yevick, J. K. *Phys. Rev.* **1958**, *110*, 1.
(27) Kotlarchyk, M.; Chen, S. H. *J. Chem. Phys.* **1983**, *79*, 2461.
(28) Willner, L.; Poppe, P.; Allgaier, J.; Monkenbusch, M.; Lindner, P.; Richter, D. *Eur. Phys. Lett.* **2000**, *51*, 628.
(29) Hamely, I.; Castelletto, V. *Prog. Polym. Sci.* **2004**, *29*, 909.
(30) Svensson, B.; Olsson, U.; Alexandridis, P.; Mortensen, K. *Macromolecules* **1999**, *32*, 6725.
(31) Goldmints, I.; von Gottberg, F. K.; Smith, K. A.; Hatton, T. A. *Langmuir* **1997**, *13*, 3659.
(32) Goldmints, I.; Yu, G.-E.; Booth, C.; Smith, K. A.; Hatton, T. A. *Langmuir* **1999**, *15*, 1651.
(33) Kiselev, M. A.; Lesieur, P.; Kisselev, A. M.; Lombardo, D.; Killany, M.; Lesieur, S. *J. Alloys Comput.* **2001**, *328*, 71.
(34) Caille, A. *Acad. Sci., Paris C. R.* **1972**, *274*, 891.
(35) Brotons, G.; Dubois, M.; Belloni, L.; Grillo, I.; Narayanan, T.; Zemb, T. *J. Chem. Phys.* **2005**, *123*, 024704.
(36) Ivanova, R.; Alexandridis, P.; Lindman, B. *Colloids Surf. A* **2001**, *183−185*, 41.
(37) *Handbook of Chemistry and Physics*; Weast, R., Ed.; CRC Press: Cleveland, OH **1974**.
(38) Alexandridis, P.; Olsson, U.; Lindman, B. *Macromolecules* **1995**, *28*, 7700.
(39) Alexandridis, P.; Olsson, U.; Lindman, B. *J. Phys. Chem.* **1996**, *100*, 280.
(40) Alexandridis, P.; Olsson, U.; Lindman, B. *Langmuir* **1997**, *13*, 23.
(41) Alexandridis, P.; Olsson, U.; Lindman, B. *Langmuir* **1998**, *14*, 2627.
(42) Lobry, L.; Micali, N. *Phys. Rev. E: Stat. Phys., Plasmas, Fluids, Relat.* **1999**, *60*, 7076.
(43) Mortensen, K.; Brown, W.; Jorgensen, E. *Macromolecules* **1994**, *27*, 5654.
(44) Wanka, G.; Hoffmann, H.; Ulbricht, W. *Colloid Polym. Sci.* **1990**, *268*, 101.
(45) Mortensen, K.; Brown, W.; Norden, B. *Phys. Rev. Lett.* **1992**, *68*, 2340.
(46) Alexandridis, P.; Andersson, K. *J. Phys. Chem. B* **1997**, *101*, 8103.
(47) Holmqvist, P.; Alexandridis, P.; Lindman, B. *Macromolecules* **1997**, *30*, 6788.
(48) Alexandridis, P.; Olsson, U.; Lindman, B. *Langmuir* **1996**, *12*, 1419.
(49) Aramaki, K.; Hossain, K.; Rodriguez, C.; Uddin, H.; Kunieda, H. *Macromolecules* **2003**, *36*, 9443.
(50) Armstrong, J.; Chowdhary, B.; Mitchell, J.; Beezer, A.; Lehare, S. *J. Phys. Chem.* **1996**, *100*, 1738.
(51) Evans, D. F.; Wennerstrom, H. *The Colloidal Domain*, 2nd ed.; Wiley-VCH: New York, **1999**.
(52) Alexandridis, P.; Ivanova, R.; Lindman, B. *Langmuir* **2000**, *16*, 3676.